

CHANDRA DETECTION OF THE RADIO AND OPTICAL DOUBLE HOT SPOT OF 3C 351

G.Brunetti^{1,2}, M.Bondi¹, A.Comastri³, M.Pedani⁴, S.Varano², G.Setti^{1,2}, M.J.Hardcastle⁵

Received _____; accepted _____

arXiv:astro-ph/0110227v1 9 Oct 2001

¹Istituto di Radioastronomia del CNR, via Gobetti 101, I-40129 Bologna, Italy

²Dipartimento di Astronomia, Università di Bologna, via Ranzani 1, I-40127 Bologna, Italy

³Osservatorio Astronomico di Bologna, via Ranzani 1, I-40127 Bologna, Italy

⁴Centro Galileo Galilei - S/C La Palma, 38700 TF Spain

⁵Department of Physics, University of Bristol, Tyndall Avenue, Bristol BS8 1TL, UK

ABSTRACT

In this letter we report a *Chandra* X-ray detection of the double northern hot spot of the radio quasar 3C 351. The hot spot has also been observed in the optical with the *Hubble Space Telescope* (*R*-band) and with the 3.5m. Telescopio Nazionale Galileo (*B*-band). The radio-to-optical and X-ray spectra are interpreted as the results of the synchrotron and synchrotron-self-Compton (SSC) mechanisms, respectively, with hot-spot magnetic field strengths ~ 3 times smaller than the equipartition values. In the framework of shock acceleration theory, we show that the requirement for such a relatively small field strength is in agreement with the fitted synchrotron spectral models and with the sizes of the hot spots. Finally, we show that the combination of a lower magnetic field strength with the high frequencies of the synchrotron cut-off in the fitted synchrotron spectra provides strong evidence for electron acceleration in the hot spots.

Subject headings: quasars: individual (3C351) — acceleration of particles — radiation mechanisms: non-thermal

1. INTRODUCTION

It is generally assumed that the relativistic particles in powerful radio galaxies and quasars, initially generated in the vicinity of the active galactic nucleus and channeled by the radio jets out to hundreds of kpc, are re-accelerated in the radio hot spots, which mark the location of strong planar shocks formed at the heads of the jets themselves (e.g., Begelman et al. 1984, Meisenheimer et al. 1989). One of the most important pieces of evidence in favor of electron re-acceleration in the hot spots is the detection of synchrotron

emission in the optical/near-IR band, due to high energy electrons (Lorentz factor $\gamma > 10^5$) with very short radiative lifetimes (e.g., Meisenheimer et al. 1997 and references therein). X-ray observations of non-thermal emission from the radio hot spots are of fundamental importance to constrain the energetics and the spectrum of the relativistic electrons and to test the re-acceleration scenario. Until the advent of *Chandra* non-thermal X-ray emission had only been detected from a few hot spots. One well-known detection was the *ROSAT* PSPC observation of the radio hot spots of Cygnus A (Harris et al. 1994), where the hot spot emission was interpreted as synchrotron-self-Compton (SSC) emission, implying magnetic field strengths in the hot spots close to the equipartition values. *Chandra* has enabled significant progress in this field, with a number of successful detections in the first 2 years of observations (3C 295: Harris et al. 2000; Cyg A: Wilson et al. 2000; Pictor A: Wilson et al. 2001; 3C 123: Hardcastle et al. 2001; 3C 207: Brunetti et al. 2001; 3C 263, Hardcastle et al. in prep.). With the exception of Pictor A, the best and most straightforward interpretation for the X-ray emission in these objects is provided by the SSC mechanism under approximate equipartition conditions.

In this letter we report on the *Chandra* discovery of X-ray emission from the double northern hot spot of 3C 351 (components J and L of Bridle et al. 1994) and on the modeling of the broad-band spectrum. $H_0 = 50 \text{ km s}^{-1} \text{ Mpc}^{-1}$ and $q_0 = 0.5$ are assumed throughout; 1 arcsec corresponds to 6.2 kpc at the redshift of 3C 351. Reported errors are at the 90% confidence level.

2. TARGET AND DATA ANALYSIS

The powerful double-lobed radio source 3C 351 is identified with a quasar at a redshift $z = 0.371$ (Laing et al. 1983). In addition to the *Chandra* data, we have analyzed Very Large Array (VLA) and *HST* archive data and obtained new *B*-band observations with the

3.5m Telescopio Nazionale Galileo (TNG).

2.1. Radio and optical data

Table 1 lists the observations used in this paper and the derived flux densities at different frequencies. The 1.4 GHz values are derived from an A+B-configuration VLA image published by Leahy & Perley (1991). Excellent high-resolution deep radio images at 5 GHz have been published by Bridle et al. (1994), and the 5-GHz flux density of 3C 351–J is from this paper. Higher frequency radio fluxes have been obtained by reducing archive VLA observations at 15 and 22 GHz. Standard procedures for calibration and deconvolution were applied to the data. The fluxes of the hot spots were corrected for primary beam attenuation and for atmospheric opacity.

Röser (1989) first discovered the northern radio hot spots in the optical band, whereas Lähteenmäki & Valtaoja (1999) found optical linear polarisation (*I*- and *V*-band) with the 2.5 m Nordic Optical Telescope on La Palma; to our knowledge, no optical fluxes have been quoted in the literature. On 1995 November 29, 3C 351 was observed with the WFPC2 on the *HST* for 2400 s using the filter F702W (close to *R*-band). We analyzed these *HST* observations in the standard manner, removing cosmic rays and using the bright quasar nucleus to correct the astrometry. On the basis of positional coincidence we identified optical counterparts of the two northern radio hot spots on the WFPC2 image. In order to better constrain the optical spectra we also observed these hot spots with a 1200-s B-band exposure at the 3.5m TNG on La Palma during the night of 2001 August 16. The hot spots were detected with a high signal to noise and the errors on the fluxes (Table 1), obtained with 4-arcsec aperture photometry (the seeing was 1.5 arcsec), are within 10%.

2.2. X-ray data

We have analyzed archival data on 3C 351 observed for 9.8 ks with the *Chandra* observatory on 2000 June 1 in GTO time. The raw level 1 data were re-processed using the latest version (CIAO2.1) of the CXCDS software. We generated a clean data set by selecting the standard grades (0,2,3,4,6) and energies in the band 0.1–10 keV. The X-ray image is shown in Fig. 1, with superimposed contours of the 1.4-GHz VLA radio image. In addition to the nuclear source, two relatively bright X-ray sources, coincident with the double northern radio hot spot, are clearly detected: $\sim 82 \pm 10$ and 54 ± 9 net counts are associated with components J and L, respectively. Despite the poor statistics, we have attempted to derive spectral information using appropriate response and effective area functions. In both cases a single power law (3C 351–J: $\alpha = 1.2 \pm 0.5$; 3C 351–L: $\alpha = 1.7 \pm 1.2$), with absorption fixed at the Galactic value $N_{\text{H}} = 2.26 \times 10^{20} \text{cm}^{-2}$ (Elvis et al. 1989), provides an acceptable description of the data.

3. EMISSION PROCESSES AND ELECTRON ACCELERATION

3.1. Modeling the broad band spectrum

As no bright thermal emission from a cluster around 3C 351 has been detected by the *Chandra* observation, we find that X-ray emission from any shocked gas in the hot spot region would be orders of magnitude lower than that observed. As discussed in the Introduction, the most plausible non-thermal mechanism responsible for X-ray emission is SSC. In Fig. 2 we show fits to the broad band spectrum of the hot spots 3C351–J and L. The emitted synchrotron and SSC spectra are obtained with standard recipes, assuming an electron energy distribution as derived under basic Fermi-I acceleration theory: a power-law spectrum with injection energy index δ which steepens at higher energies ($\gamma > \gamma_{\text{b}}$) up to

a high energy cutoff γ_c , whereas it flattens at lower energies before a low energy cutoff (equations for the electron spectrum and for the SSC calculation are given in Brunetti et al. 2001, Eqs. 2–9 and Appendix A). The SSC flux is obtained by taking radii $R_J = 0.1$ and $R_L = 0.5$ arcsec for 3C 351–J and L, respectively (Bridle et al. 1994). The parameters of the spectra obtained from fitting the radio and optical data points, i.e., the electron injection index (δ), the synchrotron break (ν_b) and cutoff frequency (ν_c) are given in Table 2 (90% confidence level). A synchrotron spectrum with a cutoff frequency at very high energies is still consistent with the data of 3C 351–J and is also plotted in Fig. 2 in order to show the maximum synchrotron contribution to the X-rays ($\leq 30\%$ at 90% confidence level). It should be noted that the high-frequency cutoff of 3C 351–J is at least one order of magnitude larger than those of other optical hot spots in the literature, and that the break frequencies for both hot spots are also higher than the typical breaks measured in the synchrotron spectra of optical hot spots (e.g., Meisenheimer et al. 1997; Gopal-Krishna et al. 2001).

We find that for both hot spots the SSC mechanism provides a good representation of the *Chandra* data for magnetic fields, (B_{ic} , Table 2), which are a factor of ~ 3 smaller than the equipartition values ($B_{eq} \simeq 230 \mu\text{G}$ for 3C 351–J and $B_{eq} \simeq 100 \mu\text{G}$ for 3C 351–L). For these field strengths, we find that inverse-Compton (IC) scattering of cosmic microwave background (CMB) photons could account for $\sim 10\%$ of the X-ray flux of 3C 351–L, whereas it does not significantly contribute to the X-ray spectrum of 3C 351–J. It is interesting to note that the X-ray luminosity of 3C 351–J is comparable to or slightly higher than the synchrotron radio to optical luminosity. If the X-rays are of SSC origin, the radiative losses of the relativistic electrons would be dominated by IC (due to second- and third-order scattering) so that the electrons’ cooling times would be a factor of ~ 4 shorter than those due to the synchrotron process alone. However, as the value of the magnetic field strength in the Compton-dominated 3C 351–J is ~ 3 times smaller than equipartition, the radiative

cooling time of the electrons emitting synchrotron radiation at $\sim 10^{16}\text{Hz}$ is a factor ~ 2.5 larger than that computed under equipartition, so that the acceleration of such particles is eased with respect to the equipartition case. A viable model for the X-ray emission of 3C 351–J can also be obtained with a combination of a synchrotron spectrum and a SSC component (accounting for $\geq 70\%$ of the flux). In this case, the resulting spectral index would be somewhat steeper than that of the SSC model. This would imply very efficient electron acceleration processes, but the basic SSC model remains unchanged. Improved spectral measurements may be able to settle the size of a possible synchrotron contribution.

Relativistic boosting appears to be necessary to explain the X-ray jet emission in a few core-dominated radio-loud quasars (e.g., Tavecchio et al. 2000; Celotti et al. 2001; Brunetti et al. 2001), however its role in the case of the hot spots is still unclear; for instance, statistical analysis of samples of FR II radio sources implies non-relativistic velocities (e.g., Arshakian & Longair 2000). Under equipartition (in the hot spot frame) IC scattering of CMB photons can produce the observed X-ray fluxes for Doppler factors $\mathcal{D} \sim 8$ and 3.8 in the cases of 3C 351–J and L, respectively. Such factors, however, can only be obtained for relatively small angles between the hot spots’ velocities and the line of sight ($\theta \leq 6^\circ$ with $\Gamma_{\text{bulk}} > 4$ for 3C 351–J, and $\theta \leq 15^\circ$ with $\Gamma_{\text{bulk}} > 2$ for 3C 351–L), whereas the radio properties of 3C 351 and the lack of lobe asymmetry suggest much larger inclination angles and smaller hot spot velocities. This problem remains even if we relax the equipartition condition: assuming a departure from equipartition similar to that required by the SSC, a Doppler factor $\mathcal{D} \sim 4.5$ ($\theta \leq 10^\circ$) is necessary to match the X-ray flux of 3C 351–J by IC scattering of the CMB. A second possible way of accounting for the large X-ray fluxes of the hot spots is to require the SSC to be enhanced with respect to the synchrotron emission via Doppler de-boosting. We find, however, that in order to match the data under equipartition conditions $\mathcal{D} \sim 0.25$ is required, implying extremely high bulk Lorentz factors ($\Gamma_{\text{bulk}} \sim 15 - 30$, with $\theta \sim 30 - 40^\circ$).

3.2. Is *in situ* re-acceleration necessary ?

Based on evidence for relativistic jet bulk motion out to 100-kpc scales, Gopal-Krishna et al. (2001) have reconsidered a minimum loss scenario in which the relativistic electrons, accelerated in the central active nucleus, flow along the jets losing energy only due to the inescapable IC scattering of CMB photons. Under these assumptions, comparing the electron radiative lifetime with the travel time to the hot spots, they find that *in situ* electron re-acceleration is in general not absolutely necessary to explain the optical/near-IR synchrotron radiation from the hot spots so far detected. Following Gopal-Krishna et al. (2001) we define $\eta = D_{\text{obs}}/D_{\text{max}}$, the ratio between the distance of the hot spots from the nucleus and the largest distance covered by the electrons in the jet before dropping to less than e^{-1} of their initial energy due to IC losses; i.e.,

$$D_{\text{max}}(\text{kpc}) \simeq 145 \frac{\beta_{\text{bulk}} \sin \theta}{\Gamma_{\text{bulk}}(1+z)^{4.5}} \left[\frac{B(\mu\text{G})}{\nu_c(10^{14}\text{Hz})} \right]^{1/2} \quad (1)$$

With $\theta \sim 30^\circ$ and our constraints on ν_c and B we find $\eta \geq 26$ –110 (3C 351–J) and $\eta \sim 9$ –38 (3C 351–L) for $\Gamma_{\text{bulk}} = 2$ –10 (as adopted by Gopal-Krishna et al. 2000). We also find that if the electrons are accelerated in 3C 351–J and then transported in a jet out to 3C 351–L, the lifetime of the optically emitting electrons in 3C 351–L ($\sim 5 \times 10^4$ yr assuming $B \geq 10\mu\text{G}$ in the jet) is at least one order of magnitude less than the time necessary to cover the distance between the two hot spots at non-relativistic speeds, and η is still > 2.2 if they are transported at relativistic speeds. These large values unequivocally point to the necessity of efficient re-acceleration processes in both the northern hot spots of 3C 351.

3.3. Electron acceleration in the hot spot

An independent estimate of the magnetic field strength B in the hot spot can be obtained in the framework of shock acceleration models. The highest energies of the relativistic electrons accelerated in a shock region by Fermi processes is given by the ratio between gain and loss terms. For a strong shock (here, for simplicity, we consider the non-relativistic case) the largest energy of the accelerated electrons is (e.g., Meisenheimer et al. 1989):

$$\gamma_c \propto u_-^2 B_+^{-2} \lambda_+(B_+)^{-1} \quad (2)$$

where u_- is the velocity of the flow in the upstream region (with respect to the shock), $B_+ = \sqrt{B_{ic}^2 + B^2}$ is the total equivalent magnetic field strength in the downstream region, and $\lambda_+(B_+)$ is the mean free path of the relativistic electrons in the downstream region.

The break energy of the electrons in the downstream region (i.e., the highest energy of the oldest electrons in the post shock region) is:

$$\gamma_b = \frac{\gamma_c}{1 + C \frac{l}{u_+} B_+^2 \gamma_c} \propto \frac{u_+}{l} B_+^{-2} \quad (3)$$

where u_+ is the velocity of the flow in the downstream region, l is the linear extension of such a region and C a constant. Substituting into Eqs.(2–3) the expression for the synchrotron cutoff frequency, $\nu_c \propto \gamma_c^2 B$, one obtains:

$$B_+ \sim 2.3 \left(\frac{u_+}{0.3} \left[\frac{\gamma_c}{\gamma_b} - 1 \right] \right)^{2/3} l_{\text{kpc}}^{-2/3} \left(\frac{\nu_c}{10^{15} \text{Hz}} \right)^{-1/3} \xi^{1/3} \quad (4)$$

where $\xi = B/B_+$ is $\simeq 0.5$ for the hot spot J and 0.9 for L, and the value of l_{kpc} can be estimated from Bridle et al. (1994). For $\gamma_c/\gamma_b \gg 1$ Eq.4 reduces to $B_+ \propto \nu_b^{-1/3}$, and from

the values of ν_b previously constrained we find $B \sim 80$ and $30\mu\text{G}$ for J and L, respectively, with a formal uncertainty of about a factor 2. These values are in good agreement with the magnetic field strengths implied by an SSC origin for the X-ray emission.

4. CONCLUSIONS

The radio to optical spectrum of the two northern hot spots of 3C 351 is well accounted for by a synchrotron model under the standard shock acceleration scenario. The most straightforward interpretation of the X-ray emission discovered by *Chandra* is the SSC mechanism. A viable model for 3C 351–J is also given by a combination of SSC and synchrotron spectra, with the SSC accounting for $\geq 70\%$ of the X-ray flux. In order to match the X-ray fluxes a magnetic field strength of a factor 3 lower than the equipartition value is required in both the hot spots. In principle the assumption of relativistic bulk motion of the hot spots might reduce the departure from equipartition, but large *ad hoc* distortions of the radio jet would be required, with the hot spots moving close to the line of sight. The frequencies of the cutoff in the synchrotron spectra and the magnetic field strengths point to the need for *in situ* electron (re)acceleration in the region of both the hot spots. When we independently estimate the magnetic field strength of the hot spots, using relationships from standard shock theory, our results are consistent with the more precise value obtained by modeling the X-ray emission as resulting from the SSC mechanism.

This work is partially supported by the Italian Ministry for University and Research (MURST) under grant Cofin99-02-37 and Cofin00-02-36. This paper is based on observations made with the Italian Telescopio Nazionale Galileo (TNG) operated on the island of La Palma by the Centro Galileo Galilei of the CNAA at the Spanish Observatorio del Roque de los Muchachos of the Instituto de Astrofísica de Canarias. We would like to

thank R. Fanti for very useful discussions and A. Zacchei for technical support.

REFERENCES

- Arshakian, T. G., Longair, M. S. 2000, MNRAS, 311, 846
- Begelman, M. C., Blandford, R., Rees, M. J. 1984, Rev. Mod. Phys., 56, 255
- Bridle, A. H., Hough, D. H., Lonsdale, C. J., Burns, J. O., Laing, R. A. 1994, AJ, 108, 766
- Brunetti, G., Bondi, M., Comastri, A., Setti, G. 2001, A&A, submitted
- Celotti, A., Ghisellini, G., Chiaberge, M. 2001, MNRAS, 321, L1
- Elvis, M., Lockman, F.J., Wilkes, B.J. 1989, AJ, 97, 777
- Gopal-Krishna, Subramanian, P., Wiita, P. J., Becker, P. A. 2001, A&A, submitted;
astro-ph/0108144
- Hardcastle, M. J., Birkinshaw, M., Worrall, D. M. 2001, MNRAS, 323, L17
- Harris, D. E., Carilli, C. L., Perley, R. A. 1994, Nature, 367, 713
- Harris, D. E., Nulsen, P. E. J., Ponman, T. J., Bautz, M., Cameron, R. A., et al. 2000,
ApJ, 530, L81
- Lähteenmäki, A., Valtaoja, E. 1999, AJ, 117, 1168
- Laing, R. A., Riley, J. M., Longair, M. S. 1983, MNRAS, 204, 151
- Leahy, J. P., Perley, R. A. 1991, AJ, 102, 537
- Meisenheimer, K., Röser, H.-J., Hiltner, P. R., Yates, M. G., Longair, M. S., et al. 1989,
A&A, 219, 63
- Meisenheimer, K., Yates, M. G., Roeser, H.-J. 1997, A&A, 325, 57

Röser, H.-J. 1989, in Lecture Notes in Physics 327, Hot Spots in Extragalactic Radio Sources, ed. K.Meisenheimer, H.-J. Röser (Berlin Heidelberg: Springer-Verlag), 91

Tavecchio, F., Maraschi, L., Sambruna, R. M., Urry, C. M. 2000, ApJ, 544, 23

Wilson, A. S., Young, A. J., Shopbell, P. L. 2000, ApJ, 544, L27

Wilson, A. S., Young, A. J., Shopbell, P. L. 2001, ApJ, 547, 740

Table 1: Observations

Band	Freq	Telescope	Flux J mJy	Flux L mJy
Radio	1.4	VLA A+B	480 ^a	1290 ^a
	4.9	VLA A+B	201 ^b	
	15.0	VLA C	85	219
	22.0	VLA C	72	174
Optical	R	HST	2.5E-3	3.8E-3
	B	TNG	1.5E-3	1.3E-3
X-ray	1 keV	<i>Chandra</i>	5.2±1.1E-6	3.4±1.1E-6

^a Leahy & Perley (1991), ^b Bridle et al. (1994). Errors on radio fluxes (1.4 to 15 GHz) are within 5%, whereas those on 22 GHz and optical fluxes are within 10%.

Table 2: Spectral parameters and B -fields

Hot Spot	δ	ν_b (10 ¹³ Hz)	ν_c (10 ¹⁴ Hz)	B_{ic} (μ G)
L	2.5	3.6±3.0	11±7	35
J	2.4	0.35±0.25	≥90	70

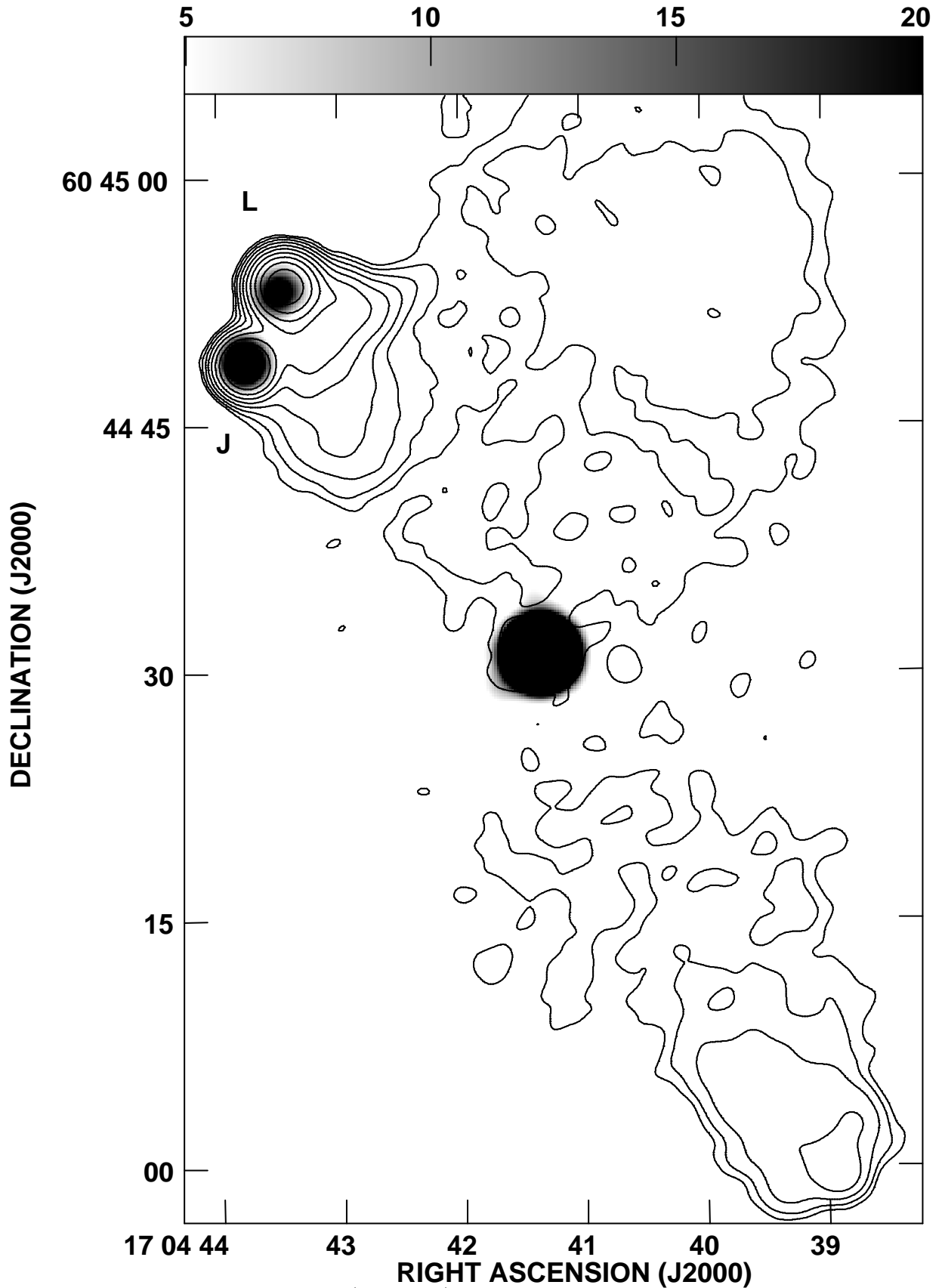


Fig. 1.— The 1.4 GHz VLA data (contours) overlaid on the 0.3–8 keV ACIS *Chandra* image (grey scale). The radio contours are : $1.0 \times (-1, 1, 2, 4, \dots)$ mJy/beam; beam=1.85 arcsec.

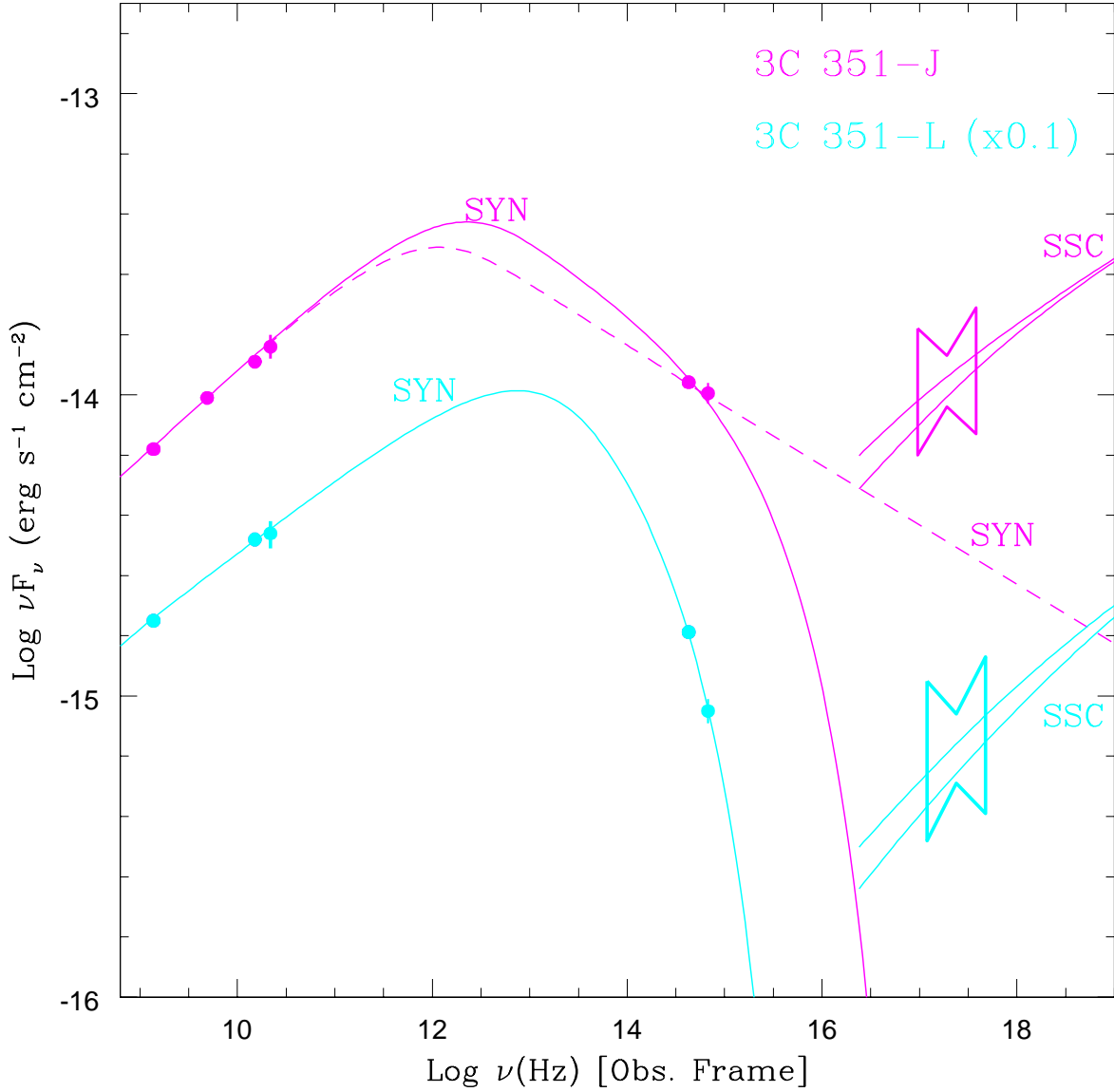


Fig. 2.— Synchrotron and SSC models (solid lines) compared with the data of 3C 351–J (magenta) and L (cyan). 3C 351–J: the synchrotron model (solid line) has $\delta = 2.4$, $\nu_b = 3.2 \times 10^{12} \text{Hz}$ and $\nu_c = 1.2 \times 10^{16} \text{Hz}$. The corresponding SSC models are calculated with $B = 70 \mu\text{G}$ and with a low frequency cutoff in the synchrotron photons at 100 MHz (lower curve) and 1 MHz (upper curve). A synchrotron model with $\nu_b = 1.6 \times 10^{12} \text{Hz}$ and no cutoff is also shown (dashed line). 3C 351–L: the synchrotron model has $\delta = 2.5$, $\nu_b = 2.2 \times 10^{13} \text{Hz}$ and $\nu_c = 1.1 \times 10^{15} \text{Hz}$, the corresponding SSC models are calculated with $B = 35 \mu\text{G}$, with the other parameters as in the case of 3C 351–J. The fluxes of 3C 351–L are reported in the panel multiplied by a factor 0.1